

$\tau$  physics at LHCb

JON HARRISON

*School of Physics and Astronomy  
The University of Manchester, M13 9PL, UK*

We report on the first searches for lepton flavour violating  $\tau^-$  decays at a hadron collider. These include searches for the lepton flavour violating decay  $\tau^- \rightarrow \mu^+ \mu^- \mu^-$  and the lepton flavour and baryon number violating decays  $\tau^- \rightarrow \bar{p} \mu^+ \mu^-$  and  $\tau^- \rightarrow p \mu^- \mu^-$ . Upper limits of  $\mathcal{B}(\tau^- \rightarrow \mu^+ \mu^- \mu^-) < 4.6 \times 10^{-8}$ ,  $\mathcal{B}(\tau^- \rightarrow \bar{p} \mu^+ \mu^-) < 3.4 \times 10^{-7}$  and  $\mathcal{B}(\tau^- \rightarrow p \mu^- \mu^-) < 4.6 \times 10^{-7}$  are set at 90% confidence level. A measurement of the inclusive  $Z \rightarrow \tau^+ \tau^-$  cross-section at 7 TeV is also reported and is found to be consistent with the Standard Model. The ratio of the  $Z \rightarrow \tau^+ \tau^-$  cross-section to the  $Z \rightarrow \mu^+ \mu^-$  cross-section is found to be consistent with lepton universality.

PRESENTED AT

The 7th International Workshop on Charm Physics  
(CHARM 2015)  
Detroit, MI, 18-22 May, 2015

# 1 $\tau$ lepton flavour and baryon number violation

## 1.1 Introduction

Lepton flavour violating (LFV) processes are allowed within the context of the Standard Model (SM) with massive neutrinos, albeit with vanishingly small branching fractions. Many New Physics (NP) models allow for enhanced rates which approach current experimental sensitivities in certain regions of parameter space [1]. Setting limits on the branching fractions of such decays helps to constrain these models, whilst a direct observation of charged LFV would be a clear sign of NP.

At the LHCb experiment [2], the inclusive  $\tau^-$  production cross-section\* is large, such that in one nominal year of data taking a factor of  $\sim 100$  more  $\tau^-$  leptons are produced than in the total samples collected over the lifetimes of the BaBar and Belle experiments. This, combined with the clean detector signatures provided by final-state muons, makes searches for decays such as  $\tau^- \rightarrow \mu^+ \mu^- \mu^-$  particularly promising. The current world's best limit on the branching fraction for  $\tau^- \rightarrow \mu^+ \mu^- \mu^-$  is  $2.1 \times 10^{-8}$  at 90% confidence level (CL) from Belle [3].

The physics reach of these searches can be further extended by considering decays such as  $\tau^- \rightarrow \bar{p} \mu^+ \mu^-$  and  $\tau^- \rightarrow p \mu^- \mu^-$ , which are also baryon number violating and lepton number violating, whilst still containing multiple final-state muons. These decays both have  $\Delta(B - L) = 0$  ( $B$  and  $L$  are the net baryon number and lepton number respectively), as required by most extensions of the SM, but could have rather different NP interpretations [4]. No measurements for these decays currently exist, but complementary searches such as  $\tau^- \rightarrow \Lambda h^-, \bar{\Lambda} h^-$  (with  $h = \pi, K$ ) have been performed by BaBar and Belle, with limits of order  $10^{-7}$  obtained [5].

In the following we describe the searches for  $\tau^- \rightarrow \mu^+ \mu^- \mu^-$ ,  $\tau^- \rightarrow \bar{p} \mu^+ \mu^-$  and  $\tau^- \rightarrow p \mu^- \mu^-$  decays [6, 7] using samples of proton-proton collisions collected at  $\sqrt{s} = 7$  TeV in 2011 and  $\sqrt{s} = 8$  TeV in 2012. For the  $\tau^- \rightarrow \bar{p} \mu^+ \mu^-$  and  $\tau^- \rightarrow p \mu^- \mu^-$  analyses only the 7 TeV dataset is used, which corresponds to an integrated luminosity of  $1.0 \text{ fb}^{-1}$ . For the  $\tau^- \rightarrow \mu^+ \mu^- \mu^-$  analysis the addition of the 8 TeV sample gives a combined integrated luminosity of  $3.0 \text{ fb}^{-1}$  and supercedes the results from Ref. [6].

## 1.2 Event selection

After passing the LHCb trigger [8], candidates are selected with loose cuts based on the kinematics of the reconstructed particles. For the  $\tau^- \rightarrow \bar{p} \mu^+ \mu^-$  and  $\tau^- \rightarrow p \mu^- \mu^-$  channels loose particle identification (PID) requirements are also applied. As the analysis is performed blind, initially candidates within  $\pm 30 \text{ MeV}/c^2$  of  $m_\tau$  are excluded.

---

\*The inclusion of charge conjugate processes is implied throughout.

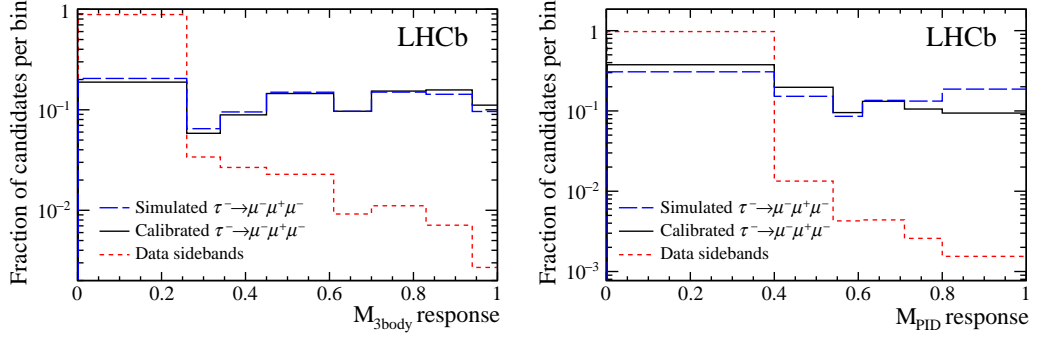


Figure 1: Response of the  $\mathcal{M}_{3\text{body}}$  (left) and  $\mathcal{M}_{\text{PID}}$  (right) likelihoods for  $\tau^- \rightarrow \mu^+ \mu^- \mu^-$  signal MC (solid and long-dashed lines) and data sideband (short-dashed lines) candidates.

In the case of  $\tau^- \rightarrow \mu^+ \mu^- \mu^-$ , the candidates are then classified according to three likelihoods,  $\mathcal{M}_{3\text{body}}$ ,  $\mathcal{M}_{\text{PID}}$  and the reconstructed invariant mass of the  $\tau^-$  candidate. The multivariate classifier  $\mathcal{M}_{3\text{body}}$  uses the kinematic and geometrical properties of the  $\tau^-$  candidate to distinguish displaced 3-body decays from  $N$ -body ( $N > 3$ ) and combinations of tracks from different vertices. The multivariate classifier  $\mathcal{M}_{\text{PID}}$  quantifies the compatibility of each of the three decay products with the muon hypothesis, using information from the Ring Imaging Cherenkov detectors, calorimeters and muon stations. Both classifiers are trained on signal and background (inclusive  $b\bar{b}$  and inclusive  $c\bar{c}$ ) Monte Carlo (MC) and are calibrated on  $D_s^- \rightarrow \phi(\mu^+ \mu^-) \pi^-$  and  $J/\psi \rightarrow \mu^+ \mu^-$  data respectively. The data is binned in bins of  $\mathcal{M}_{3\text{body}}$  and  $\mathcal{M}_{\text{PID}}$ , and the number of bins and the position of the bin boundaries in each classifier are optimised, depending on the classifier and the data taking year. Figure 1 shows the response of  $\mathcal{M}_{3\text{body}}$  and  $\mathcal{M}_{\text{PID}}$  for  $\tau^- \rightarrow \mu^+ \mu^- \mu^-$  signal MC and data outside of the signal region, which is referred to in the following as the data sidebands. For invariant mass classification the signal shape in the mass window is taken from a fit to  $D_s^- \rightarrow \phi(\mu^+ \mu^-) \pi^-$  events in data, shown in Figure 2 for 8 TeV data with the  $\tau^- \rightarrow \mu^+ \mu^- \mu^-$  selection. Both the central value of the mass window and the mass resolution are corrected according to the measured scaling and resolution in data at LHCb.

For  $\tau^- \rightarrow \bar{p} \mu^+ \mu^-$  and  $\tau^- \rightarrow p \mu^- \mu^-$  the candidates are classified according to  $\mathcal{M}_{3\text{body}}$  and the invariant mass of the  $\tau^-$  candidate, in an identical manner to  $\tau^- \rightarrow \mu^+ \mu^- \mu^-$ . Particle identification requirements are then imposed through the application of hard cuts on the inputs to  $\mathcal{M}_{\text{PID}}$  to separate protons from pions and muons from charged hadrons.

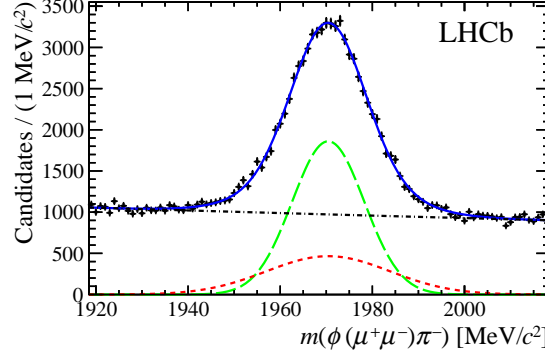


Figure 2: Invariant mass distribution of  $D_s^- \rightarrow \phi(\mu^+\mu^-)\pi^-$  candidates in 8 TeV data. The solid line shows the overall fit, the long-dashed and short-dashed lines show the two Gaussian components of the  $D_s^-$  signal and the dot-dashed line shows the combinatorial background contribution.

### 1.3 Normalisation

The observed number of  $\tau^- \rightarrow \mu^+\mu^-\mu^-$ ,  $\tau^- \rightarrow \bar{p}\mu^+\mu^-$  or  $\tau^- \rightarrow p\mu^-\mu^-$  candidates is converted into a branching fraction by normalising to the  $D_s^- \rightarrow \phi(\mu^+\mu^-)\pi^-$  calibration channel according to

$$\mathcal{B}(\tau \rightarrow X\mu\mu) = \mathcal{B}(D_s \rightarrow \phi(\mu\mu)\pi) \times \frac{f_\tau^{D_s}}{\mathcal{B}(D_s \rightarrow \tau\nu_\tau)} \times \frac{\epsilon_{D_s \rightarrow \phi\pi}}{\epsilon_{\tau \rightarrow X\mu\mu}} \times \frac{N_{\tau \rightarrow X\mu\mu}}{N_{D_s \rightarrow \phi\pi}}.$$

The branching fraction of  $D_s^- \rightarrow \phi(\mu^+\mu^-)\pi^-$  is determined from known branching fractions taken from Ref. [9]. The branching fraction of  $D_s^- \rightarrow \tau^-\nu_\tau$  is also taken from Ref. [9]. The quantity  $f_\tau^{D_s}$  is the fraction of  $\tau^-$  that come from  $D_s^-$  decays, calculated using the  $b\bar{b}$  and  $c\bar{c}$  cross-sections as measured by LHCb [10, 11], the inclusive  $b \rightarrow \tau^-$  and  $c \rightarrow \tau^-$  rates as measured by the LEP experiments and various branching fractions from Ref. [9]. This term is required as  $D_s^- \rightarrow \tau^-\nu_\tau$  only accounts for  $\sim 80\%$  of the production of  $\tau^-$  leptons. The total efficiencies,  $\epsilon_{\tau \rightarrow X\mu\mu}$  and  $\epsilon_{D_s \rightarrow \phi\pi}$ , take into account the acceptance, selection and trigger efficiencies for the signal and normalisation channels, whilst  $N_{D_s \rightarrow \phi\pi}$  is the number of reconstructed  $D_s^- \rightarrow \phi(\mu^+\mu^-)\pi^-$  events in data, and  $N_{\tau \rightarrow X\mu\mu}$  is the observed number of signal events.

For  $\tau^- \rightarrow \bar{p}\mu^+\mu^-$  and  $\tau^- \rightarrow p\mu^-\mu^-$  the normalisation is identical, aside from the inclusion of the PID cut efficiencies in  $\epsilon_{\tau \rightarrow p\mu\mu}$  and  $\epsilon_{D_s \rightarrow \phi\pi}$ . The tight PID requirements result in a larger normalisation factor, but a reduced background level, such that the overall effect is similar to the use of the multivariate classifier.

The advantage of the relative normalisation is that many of the systematic errors that are common to both the signal and normalisation channels cancel and an explicit knowledge of the luminosity and the inclusive  $\tau^-$  cross-section are not required.

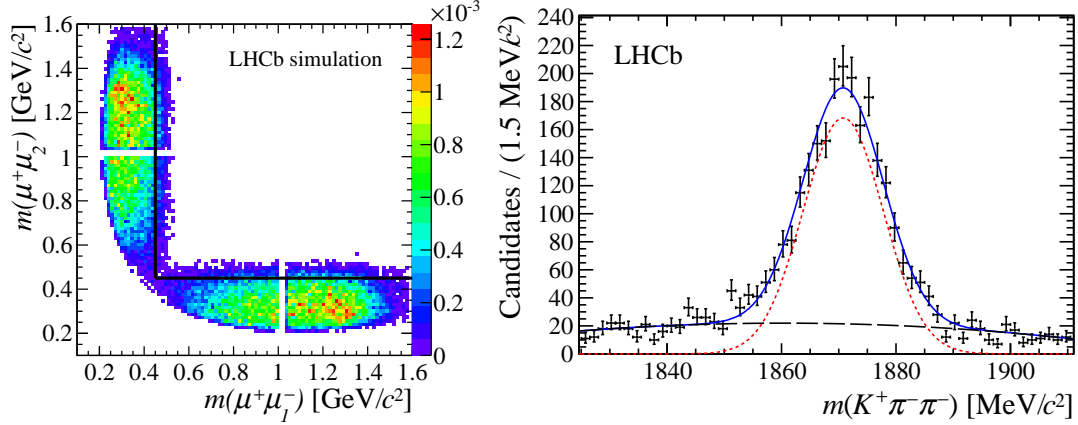


Figure 3: Left: Distribution of simulated  $D_s^- \rightarrow \eta(\mu^+\mu^-\gamma)\mu^-\nu_{\bar{\mu}}$  events as a function of dimuon mass at 8 TeV. This background is removed by excluding the regions to the left of and below the black line. Right: Fit to the 8 TeV data sidebands for the bin  $0.61 < \mathcal{M}_{3\text{body}} < 0.70$  and  $0 < \mathcal{M}_{\text{PID}} < 0.40$  under the  $K^+\pi^-\pi^-$  mass hypothesis in the  $\tau^- \rightarrow \mu^+\mu^-\mu^-$  analysis. The short-dashed and long-dashed lines indicate Gaussian and Chebychev polynomial components. These  $\mathcal{M}_{3\text{body}}$  and  $\mathcal{M}_{\text{PID}}$  bins are not used in the analysis.

## 1.4 Results

The expected number of background events per bin is calculated from an extended, unbinned maximum likelihood fit to the mass spectrum, excluding the signal region. An exponential function is used as the background probability density function for all three decays. For  $\tau^- \rightarrow \mu^+\mu^-\mu^-$  the most relevant physical background comes from  $D_s^- \rightarrow \eta(\mu^+\mu^-\gamma)\mu^-\nu_{\bar{\mu}}$  decays. About 90% of this background is removed by requiring opposite-sign dimuon masses to be greater than  $450 \text{ MeV}/c^2$ , as shown in Figure 3 (left). Backgrounds from misidentified particles such as those from  $D_{(s)}^- \rightarrow K^+\pi^-\pi^-$ , shown in Figure 3 (right), populate mainly the region of low  $\mathcal{M}_{\text{PID}}$  response and are reduced to a negligible level by the exclusion of the first bin of this likelihood. From background studies no peaking backgrounds are expected in the signal windows for  $\tau^- \rightarrow \bar{p}\mu^+\mu^-$  or  $\tau^- \rightarrow p\mu^-\mu^-$ . Fits to the invariant mass distributions in the highest likelihood bins in the data are shown in Figure 4. For  $\tau^- \rightarrow \mu^+\mu^-\mu^-$  in the final limit calculation the lowest bins in  $\mathcal{M}_{3\text{body}}$  and  $\mathcal{M}_{\text{PID}}$  are excluded as these are found not to contribute to the sensitivity.

The signal region is then unblinded and using the  $\text{CL}_s$  method [12, 13] we set observed limits at 90% (95%) CL of

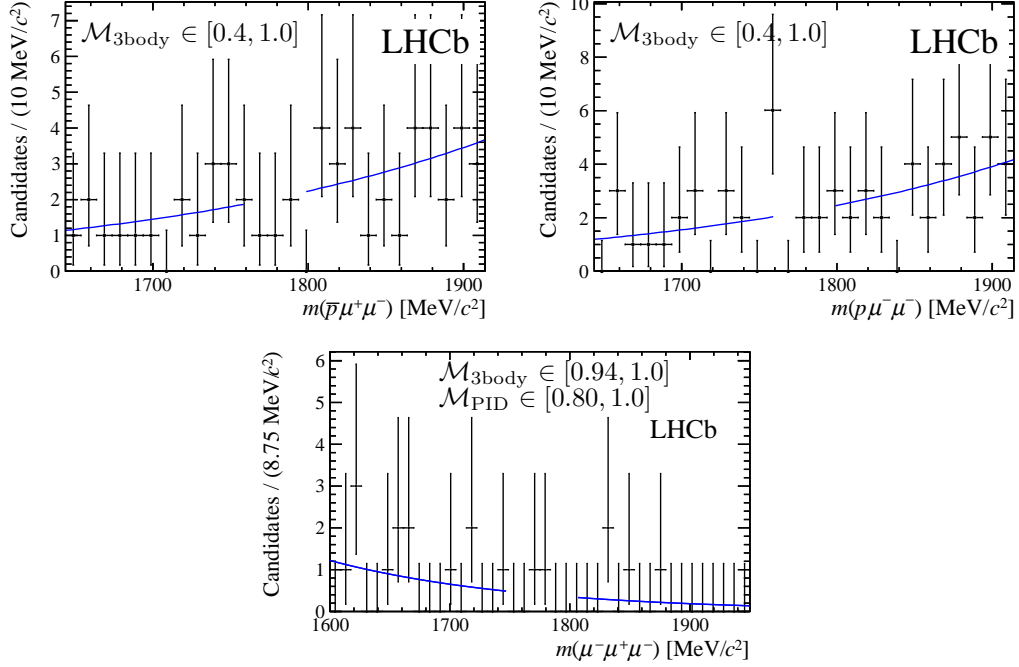


Figure 4: Fits to the mass spectra observed in the highest bins of  $\mathcal{M}_{3\text{body}}$  for  $\tau^- \rightarrow \bar{p}\mu^+\mu^-$  (top left),  $\tau^- \rightarrow p\mu^-\mu^-$  (top right) and in the highest bins of  $\mathcal{M}_{3\text{body}}$  and  $\mathcal{M}_{\text{PID}}$  for  $\tau^- \rightarrow \mu^+\mu^-\mu^-$  (bottom).

$$\begin{aligned}
\mathcal{B}(\tau^- \rightarrow \mu^+\mu^-\mu^-) &< 4.6(5.6) \times 10^{-8}, \\
\mathcal{B}(\tau^- \rightarrow \bar{p}\mu^+\mu^-) &< 3.4(4.5) \times 10^{-7}, \\
\mathcal{B}(\tau^- \rightarrow p\mu^-\mu^-) &< 4.6(6.0) \times 10^{-7}.
\end{aligned}$$

These results are the first lepton flavour violation measurements at a hadron collider. The limits for  $\tau^- \rightarrow \mu^+\mu^-\mu^-$  supercede those of Ref. [6] and, in combination with results from the  $B$  factories, improve the constraints placed on the parameters of a broad class of NP models [5]. The limits for  $\tau^- \rightarrow \bar{p}\mu^+\mu^-$  and  $\tau^- \rightarrow p\mu^-\mu^-$  represent the first ever constraints on these channels.

## 2 Inclusive $Z \rightarrow \tau^+\tau^-$ cross-section at 7 TeV

Measurements of the  $Z$  boson production cross-section are important tests of the SM. LHCb's unique coverage of the forward region allows for complementary results to those obtained from the general purpose detectors (GPDs) at the LHC. LHCb has previously published results using  $e^+e^-$  [14] and  $\mu^+\mu^-$  [15] final-states. Here,

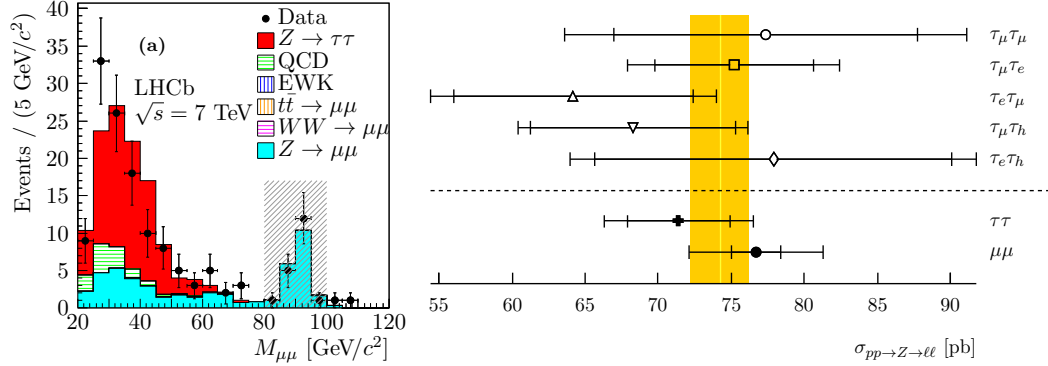


Figure 5: Left: Invariant mass distribution for the  $\tau_\mu\tau_\mu$  stream. The diagonal shaded region indicates the  $Z \rightarrow \mu^+\mu^-$  signal peak which is used to create a template for the component in the  $Z \rightarrow \tau^+\tau^-$  signal region ( $< 80 \text{ GeV}/c^2$ ). Right: Cross-sections for the  $Z$  decaying to the five streams defined in this analysis (open points) compared with theory (yellow band) and the combined  $Z \rightarrow \tau^+\tau^-$  and LHCb  $Z \rightarrow \mu^+\mu^-$  measurements (closed points). The inner error bars represent the statistical uncertainties while the outer error bars represent the total uncertainties.

measurements of the  $\tau^+\tau^-$  final-state [16] are described. These provide a verification of previous results and a test of the universal coupling of the  $Z$  to different flavours of lepton.

Using a sample of proton-proton collisions collected at  $\sqrt{s} = 7 \text{ TeV}$  in 2011, which corresponds to an integrated luminosity of  $1.0 \text{ fb}^{-1}$ , the analysis is split into five streams. These streams are denoted by  $\tau_\mu\tau_\mu$ ,  $\tau_\mu\tau_e$ ,  $\tau_e\tau_\mu$ ,  $\tau_\mu\tau_h$  and  $\tau_e\tau_h$ , depending on whether the  $\tau$  leptons decay to muons, electrons or hadrons, and require the first lepton to have  $p_T > 20 \text{ GeV}/c$  and have additional kinematic and particle identification requirements specific to each stream. Figure 5 (left) shows the invariant mass distribution for the  $\tau_\mu\tau_\mu$  stream. The QCD, electroweak, and  $Z \rightarrow \mu^+\mu^-$  backgrounds are estimated from data, whilst the  $t\bar{t}$  and  $W^+W^-$  backgrounds are estimated from simulation and are not visible.

The cross-section measurements from the individual streams are combined with the BLUE method [17] to give

$$\sigma_{pp \rightarrow Z \rightarrow \tau\tau} = 71.4 \pm 3.5 \pm 2.8 \pm 2.5 \text{ pb},$$

in the region of  $2.0 \leq \eta^\tau \leq 4.5$  with  $p_T^\tau > 20 \text{ GeV}/c$  and  $60 < M_{\tau\tau} < 120 \text{ GeV}/c^2$ . The first uncertainty is statistical, the second is systematic, and the third is due to the uncertainty on the integrated luminosity.

Figure 5 (right) shows a graphical summary of the individual final-state measurements, the combined measurement, the  $Z \rightarrow \mu^+\mu^-$  measurement of Ref. [15], and a theory prediction. The theory calculation uses DYNLO [18] with the MSTW08 next-

to-next-leading-order parton distribution functions set [19]. The results are all in good agreement.

The ratio of the combined cross-section to the LHCb  $Z \rightarrow \mu^+\mu^-$  cross-section measurement is found to be

$$\frac{\sigma_{pp \rightarrow Z \rightarrow \tau\tau}}{\sigma_{pp \rightarrow Z \rightarrow \mu\mu}} = 0.93 \pm 0.09,$$

and is consistent with lepton universality. The uncertainty is the combination of statistical, systematic, and luminosity uncertainties of the two measurements.

## References

- [1] W. J. Marciano *et al.*, Ann. Rev. Nucl. Part. Sci. **58**, 315 (2008)
- [2] LHCb collaboration, A. Alves *et al.*, JINST **3**, S08005 (2008)
- [3] Belle collaboration, K. Hayasaka *et al.*, Phys. Lett. **B 687**, 139 (2010)
- [4] M. Raidal *et al.*, Eur. Phys. J. **C 57**, 13 (2008)
- [5] Heavy Flavor Averaging Group (HFAG), Y. Amhis *et al.*, arXiv:1412.7515
- [6] LHCb collaboration, R. Aaij *et al.*, Phys. Lett. **B 724**, 36 (2013)
- [7] LHCb collaboration, R. Aaij *et al.*, JHEP **02**, 121 (2015)
- [8] R. Aaij *et al.*, JINST **8**, P04022 (2013)
- [9] Particle Data Group, K. A. Olive *et al.*, Chin. Phys. **C38**, 090001 (2014)
- [10] LHCb collaboration, R. Aaij *et al.*, JHEP **06**, 064 (2013)
- [11] LHCb collaboration, R. Aaij *et al.*, Nucl. Phys. **B 871**, 1 (2013)
- [12] A. L. Read, J. Phys. **G 28**, 2693 (2002)
- [13] T. Junk, Nucl. Instrum. Meth. **A 434**, 435 (1999)
- [14] LHCb collaboration, R. Aaij *et al.*, JHEP **02**, 106 (2013)
- [15] LHCb collaboration, R. Aaij *et al.*, JHEP **06**, 058 (2012)
- [16] LHCb collaboration, R. Aaij *et al.*, JHEP **01**, 111 (2013)
- [17] L. Lyons *et al.*, Nucl. Instrum. Meth. **A 270**, 110 (1988)
- [18] S. Catani and M. Grazzini, Phys. Rev. Lett. **98**, 222002 (2007)
- [19] A. Martin *et al.*, Eur. Phys. J. **C 63**, 189 (2009)